Effect of Graphene on Nickel Surface Relaxation: Molecular Dynamics Simulation

Sergiy Konorev *, Vitalii Yanchuk, Ivan Kruhlov, Andrii Orlov, Sergii Sidorenko, Igor Vladymyrskyi, Sergey Prikhodko, Svitlana Voloshko

Posted Date: 23 August 2023

doi: 10.20944/preprints202308.1606.v1

Keywords: molecular dynamic simulation; interplane distance; graphene; surface relaxation; surface reconstruction; packing density

Article

Effect of Graphene on Nickel Surface Relaxation: Molecular Dynamics Simulation

Sergiy Konorev [1,*], Vitalii Yanchuk [1], Ivan Kruhlov [1], Andrii Orlov [1], Sergii Sidorenko [1], Igor Vladymyrskyi [1], Sergey Prikhodko [2] and Svitlana Voloshko [1]

[1] National Technical University of Ukraine "Igor Sikorsky Kyiv Polytechnic Institute", Prospect Beresteiskyi 37, 03056 Kyiv, Ukraine; mail@kpi.ua

[2] University of California Los Angeles, 2121K-Engineering 5 420 Westwood Plaza, CA 90095-1595, USA; sergey@seas.ucla.edu

* Correspondence: konorev@kpm.kpi.ua

Abstract: The effect of graphene (GR) on Ni surface relaxation and reconstruction in three different substrate orientations: {111}, {001}, {011}, at two different temperatures: 300K and 400K was studied using Molecular Dynamics simulation. The change of the interplanar distances of the substrate and redistribution of Ni and C atoms in direction perpendicular to the surface were compared with the equilibrium state of GR and bulk Ni, in the absence of the counterpart. The surface reconstruction for GR/Ni system was analyzed base on the calculated radial pair distribution function of Ni and C atoms. The surface roughness was visualized using 2D atomic distribution maps. For the studied substrate orientations and temperatures, it was found that the most densely packed orientation of the Ni base {111} provides minimal changes of the structural parameters of both counterparts at 400 K.

Keywords: molecular dynamic simulation; interplane distance; graphene; surface relaxation; surface reconstruction; packing density

1. Introduction

Graphene (GR) is a favorable material for various applications due to the combination of its unique properties. In particular, high thermal (up to 5300 W/mK) [1, 2] and electrical conductivity (~ 10^6 S/m) [3], as well as high (97.7 %) transmittance for a broad spectrum of solar radiation [4] making GR application feasible for translucent and flexible electrodes that can be used in solar cell (SC) technologies [5]. Ideally, the SC electrode should demonstrate high transparency, low electrical resistance, chemical stability, low surface roughness, and provide all this at a reasonable cost [6]. Thus, intensive research to develop materials that meets these requirements is being carried out on carbon nanotubes [7], conductive polymers [8], metallic nanowires [9], metallic meshes [10] etc. However, GR has the best chance of outperforming in such application. It has recently been shown that due to the outstanding chemical stability of GR, its introduction into the perovskite SC can improve the functional characteristics and stability of device [11]. In addition, due to the high conductivity of GR, its addition to the front electrodes of commercially used SC on the base on indium-tin-oxide [12] and fluorine-doped-tin-oxide [13] provides significant enhancement of the device performance. Numerous studies have recently been published on the incorporation of GR in SC. Peng et al. [14] described a semitransparent perovskite SC with a multilayer GR applied to the top electrode. Yoon et al. [15] reported flexible perovskite SC with incorporated GR monolayer. Luo et al. [16] proposed a flexible perovskite SC with GR and transversely stacked carbon nanotubes used as front and rear electrodes, respectively.

Though, GR synthesis or deposition on top of metal substrate remains a challenging task, especially for some technology-relevant metals [17]. In this respect, GR surface morphology is mostly defined by the ratio of adsorption energy to the bulk cohesive energy of the substrate. When this ratio is lower, larger uniform GR islets can be formed on the metal surface [18]. Thus, a high-quality GR layer is generally easier to obtain on the Cu substrate due to the extremely low solubility of carbon

Preprints (www.preprints.org) | NOT PEER-REVIEWED | Posted: 23 August 2023 doi:10.20944/preprints202308.1606.v1

in Cu (~7 x 10^{-6} % at. 1200 K) [19]. This limited solubility causes a very low adsorption energy, which provides a relatively large GR island growth and ultimately allows a monolayer of GR to be produced and separated from the substrate [20]. However, a lattice mismatch between GR and Cu of ~10 % leads to some GR surface deformation and buckling [21]. The other substrate metals such as Au [22] and Ag [23] also demonstrate low adsorption and restrained mutual solubility with carbon, making them promising for single layer GR production. Yet, these noble metals are of high cost, which limits their technological relevance. In turn, Ni provides strong interaction [24] and good lattice matching [25] with GR. However, GR deposited on top of Ni can lead to specific relaxation and structure modifications of the near-surface layers of the substrate [26]. This inevitably modifies the functional properties of both materials and ultimately the SC device, which incorporates them. Free surface of metal is generally accepted as a 2D crystal structure defect where structure of the near surface regions can be significantly different compared to the bulk. Application of GR to the free surface of metal can significantly modify this 2D defect properties, which can be classified as surface relaxation and surface reconstruction.

In the present paper, we report results of a Molecular Dynamics simulation study of the surface structure modification of Ni induced by GR. Simulation was performed for three most closely packed crystal orientations of Ni substrate: {111}, {001}, {011} and at two different temperatures that cover the operation temperature range of SC: 300 K and 400 K.

2. Simulation procedure

The classical Molecular Dynamics approach was used in this study for simulation of Ni surface modification by numerically solving Newton's motion equations for a system of interacting particles. Forces between the particles and their potential energies were calculated using interatomic potentials for the Ni-C system, developed by Xiao et al. [27]. The LAMMPS software was used to conduct the simulation [28]. Equilibrium lattice parameters and coefficients of linear thermal expansion of Ni and GR were calculated to check the accuracy of applied interatomic potential. This simulation was conducted for defect-free atomic cell, using periodic boundary conditions in all directions. Equilibrium values of the lattice constants were determined as parameters corresponding to zero stresses of the system, while thermal expansion coefficients were calculated taking into account the average distance between neighboring atoms, not considering changes of the lattice parameters. The selected potential is considered to be appropriate in this study, which is confirmed by less than 0.4% discrepancy between simulated and reference data shown in Table 1.

Table 1. Structural parameters and coefficients of linear thermal expansion of Ni and GR calculated in this study using Molecular Dynamics simulation and corresponding reference data.

Material	Temperature, K	Lattice constant, Å		Coefficient of linear thermal expansion, 10^{-6} 1/K	
		Calculated	Reference data	Calculated	Reference data
Ni	300	3.5347	3.523 [29]	12.75	13.4 [31]
	400	3.5392			12.8 [32]
GR	300	1.4163	1.42 [30]	8.5	
	400	1.4175			

Simulation calibration and system stress analysis determine that the free surface introduces a stresses source in Ni that gradually disappears at a distance of 5 lattice periods. Therefore, the simulation cell contains a GR monolayer, 6 atomic layers of an "active" Ni and 4 atomic layers of a "frozen" Ni (Figure 1). The boundaries of the cell are fixed along the Z- axis without periodic conditions, providing free surfaces at the bottom and top of the cell. Born–von Karman boundary conditions were applied along the X- and Y-axis. The "frozen" area was introduced in order to mitigate the influence of bottom free surface. The size of this area is selected to be higher compared

Preprints (www.preprints.org) | NOT PEER-REVIEWED | Posted: 23 August 2023 doi:10.20944/preprints202308.1606.v1

to cut-off radius corresponding to interatomic potential influence range. Generally, a simulation cell is chosen with the highest possible crystal structure matching between GR and Ni.

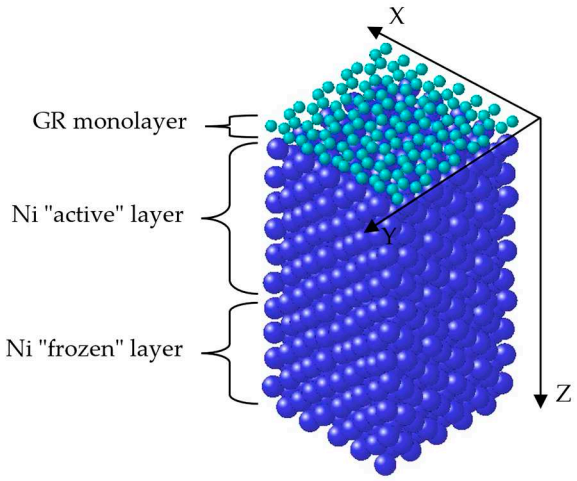

Figure 1. Schematic representation of the selected simulation cell.

The simulation time step of 10^{-15} s was selected to make sure that force and atomic positions do not change too rapidly, which was done in order to negate system instability during the simulation process due to atoms overshooting in the direction of applied force.

3. Results

3.1. Surface relaxation of Ni of various orientations with and without GR layer Subsection

The equilibrium position of an individual atom in an ideal infinite crystal is determined by the acting forces from all other atoms in the crystal, resulting in periodic structure. Laminating the surface with another material alters these forces, affecting the equilibrium positions of the remaining atoms. This changes the spacing and/or symmetry of the "active" layer of atoms compared to bulk and forms a different surface structure. These modifications in equilibrium positions of near surface atoms can be categorized as either a relaxation or a reconstruction.

The simulation results of Ni relaxation in various crystal orientations at 300 K and 400 K are given in the form of relative interplanar spacings change compared to the equilibrium bulk values (Figure 2). The selected crystal orientations of Ni were evaluated by the packing density mismatch with GR and presented in the Figure 2 in the order from smallest to largest (top-to-bottom): {111}, {001}, {011}. It is important to note that interplanar spacing modification of less than 0.5 % (Figure 2) could be considered as a temporary result of atoms thermal fluctuations and were not taken into account for the surface relaxation analysis.

Preprints (www.preprints.org) | NOT PEER-REVIEWED | Posted: 23 August 2023 doi:10.20944/preprints202308.1606.v1

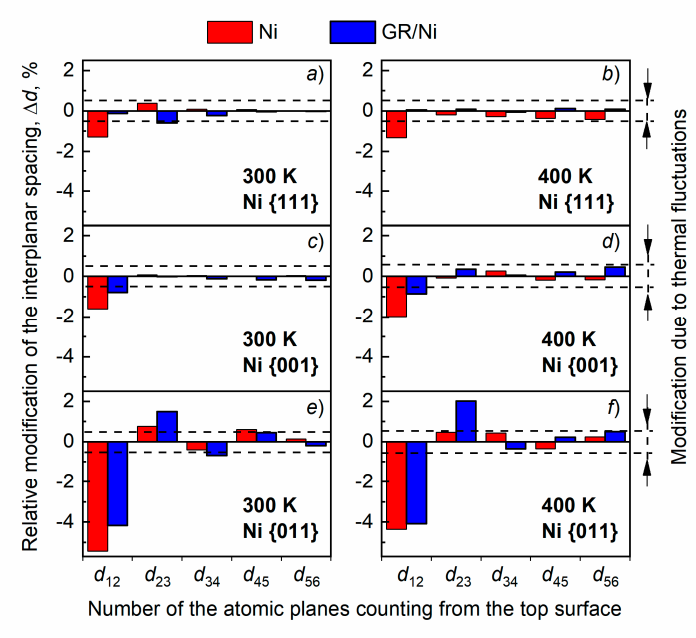

Figure 2. Interplanar spacing modification induced by Ni relaxation in {111} (a, b), {001} (c, d), and {011} (e, f) orientations with and without GR at 300 K (a, c, e) and 400 K (b, d, f).

The {111} orientation provides the most densely packed surface plane in the face-centered cubic lattice. The packing density of this plane for Ni under normal conditions of room temperature and atmospheric pressure is 1.864 x 10^{-19} atoms/m^2 [33]. For ease of analysis, the packing density in all other orientations has been correlated with respect to {111} orientation. Corresponding values were 1, 0.866, and 0.612 for {111}, {001} and {011} planes, respectively.

Ni {111}. The calculated equilibrium values of the interplanar spacing for the Ni {111} orientation in the bulk are d_b^{300} = 2.041 ± 0.001 Å and d_b^{400} = 2.043 ± 0.001 Å at 300 K and 400 K, respectively. These are well consistent with previously reported data [24]. The interplanar (d_{ij}) distances calculated using Molecular Dynamics approach were compared with d_b one: $\Delta d_{ij} = (d_b - d_{ij})/d_b$. The i and j indexes in this notation correspond to the number of the atomic layers/planes counting from the surface, e.g., d_{12} is a spacing between first and second atomic planes (Figure 3).

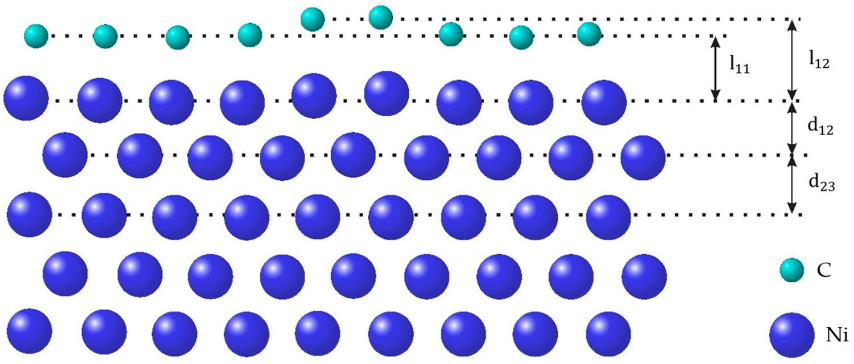

Figure 3. Transverse atomic distribution in the modeled cell.

The largest absolute interplanar spacing modifications were observed between the first and second planes: d_{12}^{300} = 2.014 ± 0.001 Å and d_{12}^{400} = 2.016 ± 0.001 Å at 300 K and 400 K, respectively. For the first interplanar spacing (d_{12}), a modification of ~ -1.3 % was observed for Ni without GR at both temperatures, as can be seen from Figure 2. Negative value of the spacing modification corresponds to the lattice compression. At 300 K the relative relaxation d_{12} changes from -1.29 % to -0.13 %, and d_{23} from 0.38 % to -0.59 % in presence of GR on top of Ni leads to the of. At 400 K, the presence of GR

Preprints (www.preprints.org) | NOT PEER-REVIEWED | Posted: 23 August 2023 doi:10.20944/preprints202308.1606.v1

almost completely eliminates the influence of the free surface, making interplanar spacing changes not exceeding 0.1 %. As a consequence, it can be assumed that on Ni {111} GR behaves like a missing Ni surface layer, negating overall surface relaxation.

Ni {001}. The calculated equilibrium values of interplanar spacing in bulk in this orientation are d_b^{300} = 1.767 ± 0.001 Å and d_b^{400} = 1.769 ± 0.001 Å at 300 K and 400 K, correspondingly, which is also well consistent with the previously reported data [34]. At 300 K, modification (Δd = -1.61 %) is observed only for the first interplanar spacing from the Ni surface (Figure 3), giving absolute calculated value of d_{12}^{300} = 1.7388 Å. Increase of the temperature up to 400 K leads to even more pronounced lattice compression (Δd = -1.99 %). Compression of -2.7 % was previously reported for this surface orientation, where it was experimentally measured using slow electrons diffraction [24].

Presence of GR on top of Ni {001} leads to the significant changes in the surface relaxation: modification of d_{12}^{300} and d_{12}^{400} interplanar spacings decreases down to -0.78 % and -0.85 %, respectively.

Ni {011}. Compared to {111} and {001} orientations, {011} has the lowest packing density, making bulk interplanar spacings of d_b^{300} = 1.250 ± 0.001 Å and d_b^{400} = 1.251±0.001 Å at 300 K and 400 K, correspondingly. Significant modification of the interplanar distance between the first two atomic planes counting from the surface was registered for this Ni orientation as well. Corresponding calculated values are d_{12}^{300} = -5.4 % and d_{12}^{400} = -4.4 %. Significant compression (-4.8 ± 1.7 %) between the first two atomic layers of Ni in this direction was also measured experimentally at room temperature and previously reported [35].

Addition of GR slightly changes the surface relaxation. The modification of the first interplanar spacing decreases down to -4.1 %, again suggesting compression. In contrast, in the case of the second distance d_{23}, it increases to 1.48 % and 2 % at 300 K and 400 K, respectively, meaning expansion.

As already mentioned, the maximum value of interplanar spacing modification was registered for all orientations in question for the d_{12}, which is first spacing from the surface. Relaxation has no impact on more than two first atomic layers of Ni. In addition, it was found that the maximum modification depends on the packing density of the plane, ranging from -1.3 % for Ni {111} (the highest packing density) to -5.4 % for Ni {011} (the lowest packing density) (Figure 4).

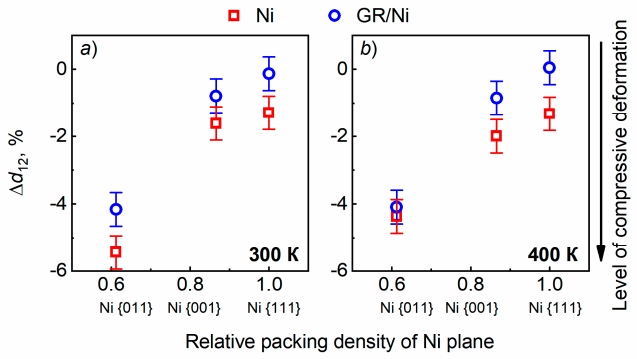

Figure 4. Change of the d_{12} interplanar spacing of Ni with and without GR at 300 K (a) and 400 K (b) as a function of atomic relative packing density.

Additionally, it was found that the temperature increase from 300 K to 400 K does not significantly affect the surface relaxation.

Finally, it was shown that GR addition lowers the influence of the free surface independent on the temperature: the maximum value of interplanar spacing modification decreases by approximately 1 % as a result of GR presence. Ni {111} plane laminated by GR reveals the smallest deviations from the bulk structure and has the smallest surface modification due to the best lattice matching, especially at 400 K.

3.2. Surface reconstruction

 doi:10.20944/preprints202308.1606.v1

Surface reconstruction is a process that changes the position of surface atoms from their equilibrium state, typical of bulk, which is accompanied by the formation of a structure that differs from bulk in periodicity and/or type of symmetry. The presence of GR on the metal surface can significantly modify reconstruction by altering both counterparts at the near surface region. To analyze the result of such a change, the radial pair distribution function (RPDF), the rearrangement of atoms in direction normal to the surface, and the 2D maps of atoms reconstruction were plotted and evaluated.

Simulation results suggest that there is no surface reconstruction of Ni in {001}, {011}, {111} orientations before introduction of GR. In this case only relaxation processes were registered. However, Ni reconstruction of the upper first atomic plane and GR occurs in addition to the relaxation process, in the presence of GR. Details of these processes are given below.

3.2.1. GR reconstruction

Structural changes of GR after its deposition on Ni in different orientations were compared to its standing alone equilibrium state. Thus, GR structure simulation was first done without Ni at 300 K and 400 K.

The RPDF, g(r) describes a probability of finding two atoms at distance r from each other. In this event, the first peak at g(r) plot characterizes a short-range ordering, and its position corresponds to an average distance between nearest atoms. Intensity of the second and other RPDF peaks allows to track the long-range ordering, while change of these peaks' positions represents structure deformation of the top plane in considered orientation.

Results of the GR structure simulation suggest that distance r between C atoms is equal to $r_{(C\text{-}C)}$ = 1,4179 ± 0.0005 Å (Figure 5a). This distance increases by 0.5 % – 0.6 % after GR deposition onto Ni in {001}, {011}, {111} orientations (Figure 5b, c, d). The second and the following RPDF peaks analysis imply GR expansion for more than 0.2 % in case of {111} orientation, and less than 0.1 % in case of {001} and {011}.

Thus, the average distance between C atoms in the deposited GR changes in 3 – 5 times higher compared to the expansion of the GR layer itself. This effect can be explained by the increased displacement of C atoms in direction perpendicular to the surface. The range of C atoms positions in this direction is characterized by Δl_C parameter. Analysis of atoms distribution in direction perpendicular to the surface allowed to determine the values: $\Delta l_C^{(Ni\ \{111\})}$ = 1,4 ± 0,05 Å, $\Delta l_C^{(Ni\ \{001\})}$ = 0,75 ± 0,05 Å, $\Delta l_C^{(Ni\ \{011\})}$ = 0,9 ± 0,05 Å for Ni orientations {111}, {001}, {011}, respectively. These values are 2 – 3 times larger compared to the GR in equilibrium state. C atoms occupy some preferred positions with different distances to the Ni surface, which are schematically illustrated in Figure 3 as l_{11} and l_{12}. This projection is confirmed by the character of the C peaks in Figure 6. For instance, presence of the shoulders in Figure 6a, b and in Figure 6e, f and doubling of peaks in Figure 6d, are clear evidence for making such account.

Temperature increase from 300 K to 400 K does not have a pronounced effect on the GR reconstruction.

Preprints (www.preprints.org) | NOT PEER-REVIEWED | Posted: 23 August 2023 doi:10.20944/preprints202308.1606.v1

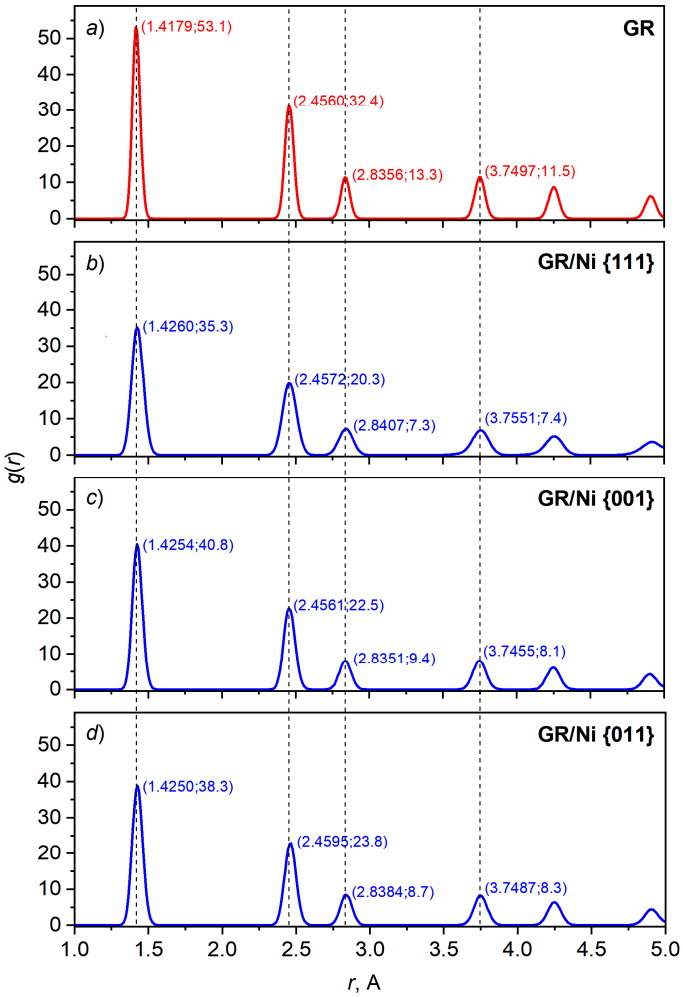

Figure 5. Radial pair distribution function g(r) for C atoms in free GR layer (a) and GR layer on the Ni surface with {111} (b), {001} (c), and {011} (d) orientations at 300 K. Position and height of the peaks are listed at their maximums.

Preprints (www.preprints.org) | NOT PEER-REVIEWED | Posted: 23 August 2023 doi:10.20944/preprints202308.1606.v1

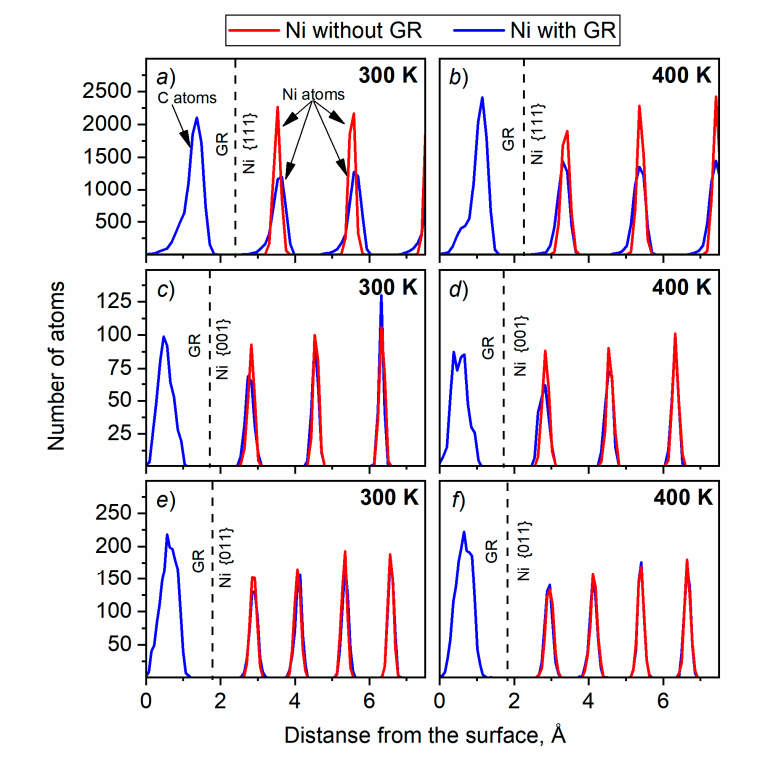

Figure 6. Distribution of atoms in direction perpendicular to the surface for {111} (a, b), {001} (c, d), and {011} (e, f) orientations of Ni with and without GR at 300 K (a, c, e) and 400 K (b, d, f).

Such inhomogeneous distribution of C atoms in direction perpendicular to the surface causes a specific surface relief. The character of this relief is determined by the orientation of Ni substrate used for GR application. This relief can be shown in 2D maps reflecting the atomic displacement perpendicular to the surface, where the displacement is color coded (Figure 7).

Preprints (www.preprints.org) | NOT PEER-REVIEWED | Posted: 23 August 2023 doi:10.20944/preprints202308.1606.v1

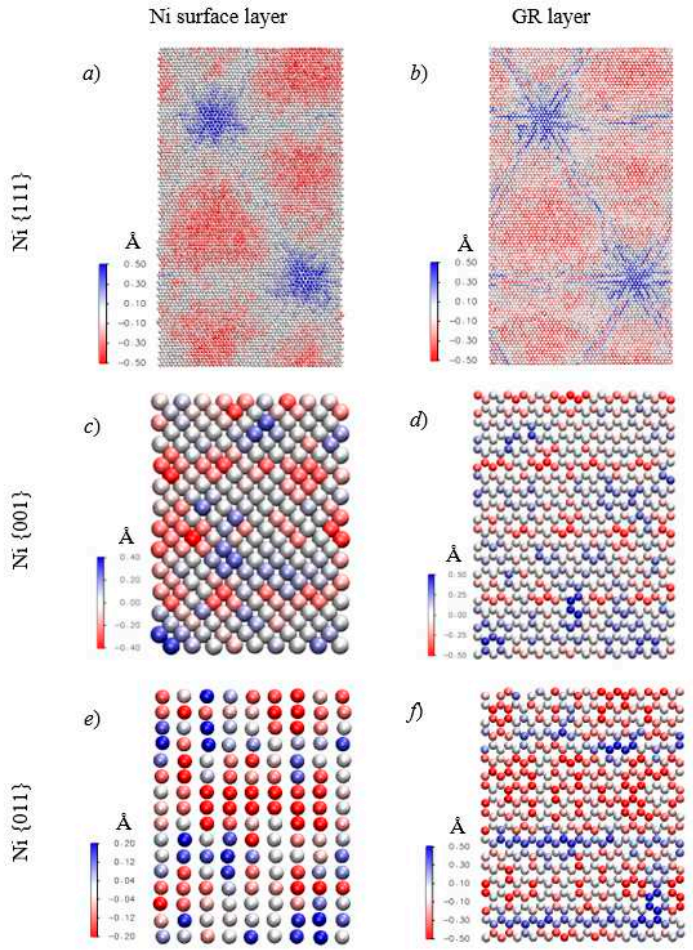

Figure 7. Maps of the atomic displacement normal to the surface; the uppermost Ni layer (a, c, e) and GR (b, d, f) at 300 K; GR/Ni {111} (a, b); GR/Ni {001} (c, d); GR/Ni {011} (e, f). The vertical offset from the average positions is given in Å.

If the crystal symmetry of the uppermost Ni layer and GR matches well, the 2D maps reveals clear periodicity, i.e. frequency of the areas limited by the same height of atoms positions (Figure 7a, b). The extent of this periodicity is about 20 – 25 atomic periods of Ni. If there is no symmetry match, the periodicity is less pronounced and reflected by the strips with a width of 4 – 5 Ni periods (Figure 7c, d, e, f).

The surface roughness of GR laminated systems can effect numerous functional properties [36, 37]. That is why the following parameters were analyzed here: R_a – an arithmetic mean deviation of the C atoms positions from the average height value; R_{max} – a maximum relief height, e.g. difference between the maximum and minimum height of atoms positions; S – an average distance between relief irregularities. It is worth noting that the integral surface roughness depends on both the height deviation and distance parameters of the surface relief, for instance the lowest roughness corresponds to the minimal R_a and R_{max} values and maximal S. Therefore, the integral S/R_a ratio was used for comparative surface relief analysis; higher S/R_a value corresponds to lower surface roughness.

Calculated surface roughness parameters of GR/Ni systems for different substrate orientations and temperatures are summarized in Table 2. The Ni {111} laminated with GR is characterized by maximum height difference (R_a and R_{max} parameters) and distance between relief irregularities (S parameter) compared to two other orientations.

Table 1. Surface roughness parameters of the GR/Ni systems depending on the Ni orientation and temperature.

Ni plane	Temperature

Preprints (www.preprints.org) | NOT PEER-REVIEWED | Posted: 23 August 2023 doi:10.20944/preprints202308.1606.v1

	300 K	400 K
{111}	R_a = 0.7 ± 0.05 Å R_{max} = 1.95 ± 0.05 Å S = 146 ± 1.4 Å S/R_a = 208	R_a = 0.55 ± 0.05 Å R_{max} = 1.75 ± 0.05 Å S = 150 ± 1.4 Å S/R_a = 272
{001}	R_a = 0.35±0.05 Å R_{max} =1.1 ± 0.05 Å S = 12 ± 1.4 Å S/R_a = 34	R_a = 0.4 ± 0.05 Å R_{max} = 1.15 ± 0.05 Å S = 13 ± 1.4 Å S/R_a = 32
{011}	R_a = 0.45 ± 0.05 Å R_{max} = 1.2 ± 0.05 Å S = 18 ± 1.4 Å S/R_a = 40	R_a = 0.55 ± 0.05 Å R_{max} =1.35 ± 0.05 Å S = 19 ± 1.4 Å S/R_a = 34

Figure 8 shows dependence of the S/R_a parameter on the relative packing density of the Ni. At 300 K the lowest roughness was found for the Ni {111} orientation, showing the maximum packing density of the surface layer. Temperature increase up to 400 K leads to the roughness decrease of the GR/Ni {111} system, giving the highest S/R_a ratio among all other cases. This effect is not observed for two other studied orientations.

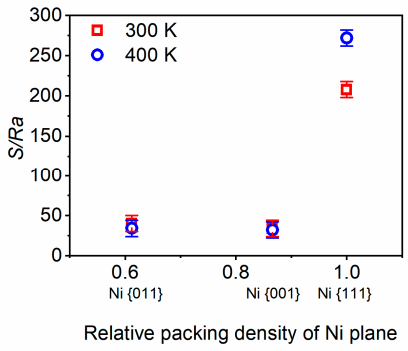

Figure 8. Dependence of the S/R_a integral surface roughness parameter on the relative packing density of the Ni atom planes and temperature.

3.2.2. Ni reconstruction

Surface reconstruction of Ni is only observed in presence of GR and only for the first atomic layer from Ni surface. RPDF provides summarized data on the structure of this Ni layer (Figure. 9). In turn, structural changes in the normal direction to the surface can be tailed from Figure 6.

Preprints (www.preprints.org) | NOT PEER-REVIEWED | Posted: 23 August 2023 doi:10.20944/preprints202308.1606.v1

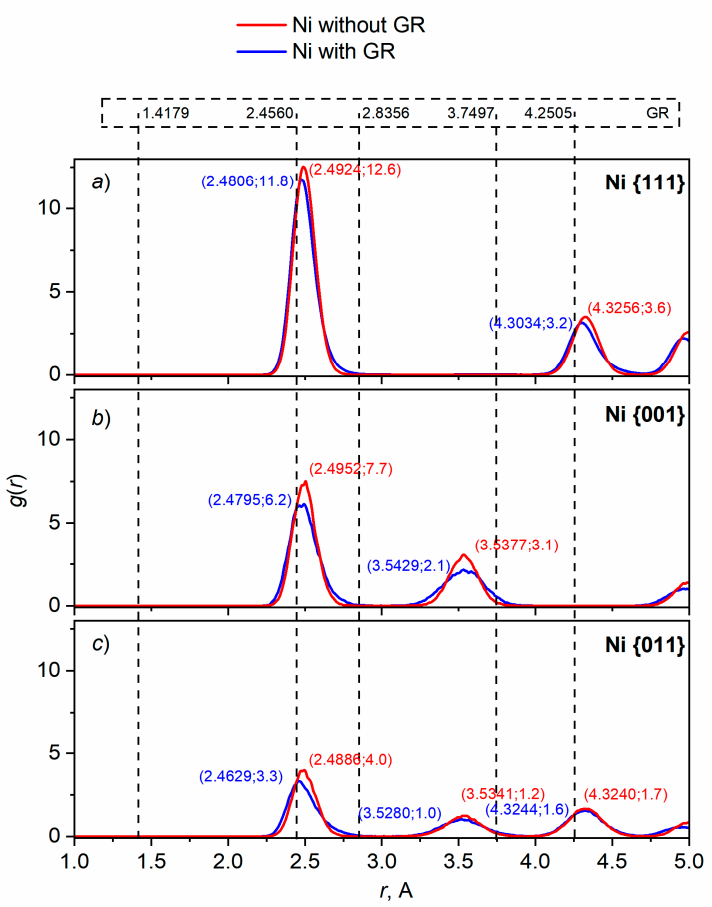

Figure 9. Radial pair distribution function g(r) for the uppermost Ni layer in {111} (a), {001} (b), and {011} (c) orientations with and without GR. Position and height of the peaks are marked at their maximums. The peaks of GR atoms are not shown but their positions are marked with dotted lines.

As follows from the analysis of the RPDF first peak position (Figure 9), an average distance between Ni atoms decreases by 0.5 %, 0.6 % and 1 % for {111}, {001} and {011} substrate orientations, respectively. According to other RPDF peak positions, the structure of the whole reconstructed Ni layer compacts not more than 0.5 % after GR deposition onto the {111} plane. There are no relative changes for the other planes (registered changes are less than 0.1 %). It should also be noted that the slight shift of Ni atoms towards the nearest C atoms shown with dotted line in Figure 9 is taking place in the presence of GR.

The character of atomic distribution in direction perpendicular to the surface (Figure 6) suggests that after lamination with GR, Ni atoms change their positions in the first atomic plane increasing the thickness of this layer by 79 %, 62 % and 42 % for {111}, {001} and {011} substrate orientations, respectively (Figure 10). Thus, increase of the plane relative packing density leads to the rise of the width of the first layer from the surface. This can be explained by the fact that for densely packed crystalline planes, atoms have more freedom to displace from their regular positions in an out-of-plane direction (perpendicular to the surface) than in-plane. Surface relief formed at various substrate orientations is shown in Figure 6a, c, e.

Preprints (www.preprints.org) | NOT PEER-REVIEWED | Posted: 23 August 2023 doi:10.20944/preprints202308.1606.v1

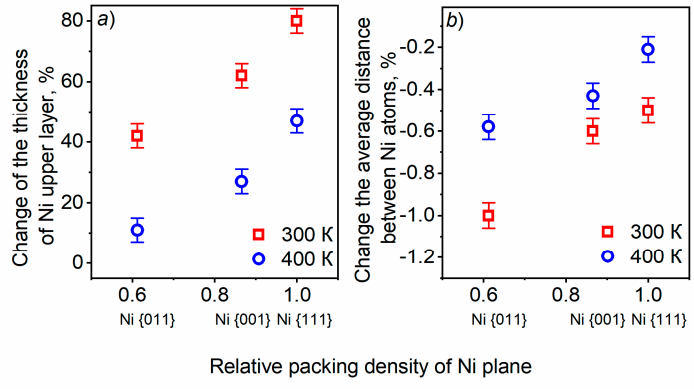

Figure 10. Dependence of the thickness variation of Ni upper layer (a) and the average distance between Ni atoms (b) on the relative packing density of Ni in presence of GR.

Temperature increase from 300 K up to 400 K for the GR/Ni system leads to lower variation of the thickness of Ni upper layer and smaller deviation of the average distance between its atoms (Figure 10). Change of the Ni upper layer thickness is lowered by ~30 % for 400 K compared to 300 K for all studied substrate orientations. Modification of the average distance between Ni atoms is also lowered for 0.2 % – 0.4 % by the absolute value. These implies a higher stability of the GR/Ni system at higher temperature. Most likely such improvement is a result of thermal expansion effect, since GR has lower coefficient of thermal expansion compared to Ni, Table 1. The Ni {111} orientation provides almost perfect matching between GR and metal lattice parameters at 400 K. Therefore, such conditions can be considered as a perfect for the lamination with GR.

4. Discussion

A few words can be said about implication of simulation results presented here. It appears that Ni surface in {111} orientation provides the best conditions for GR deposition with the temperature of substrate hold close to 400 K. The structure of the substrate in this orientation is most close to the GR. As can be seen, the surface structure of Ni restores after GR deposition in the all studied cases, i.e., impact of the free surface of Ni decreases in presence of GR. It suggests that for GR/Ni system, properties of Ni near surface layers are closer to its bulk. Another implication of this simulation is prediction of the surface roughness. It is well accepted that the oxidation of the metallic surface strongly depends on the its morphology [38]. In turn, GR shows great potential for corrosion resistance of metals (Me) [39]. Thus, it is very important to pay attention to the link between structure of the GR/Me interface and corrosion resistance [40]. Various structure defects such as wrinkles, folds, atomic defects lead to interface roughness increase with the following insertion of oxygen and water molecules from the environment. Thus, GR deformation, warpage and even the enfoldment of graphene sheets will affect corrosion properties. From this point of view, considered integral parameter S/Ra allows to analyze the roughness of metallic surfaces at different orientations and, thus, to predict their corrosion resistance. For instance, this parameter values are different for 8.5 times for Ni {111} and {011} orientations at 400 K. However, calculated roughness values are quite small suggesting that GR could provide stable corrosion protection in all considered cases. Sufficient enhancement of corrosion characteristics of the GR/Ni system compared to free Ni could be predicted as well. Of course, this simulation rather presents an ideal case of GR deposition on Ni single crystal defect-free surface. For sure, defects of both Ni (vacancies, grain boundaries, triple junctions, etc.) and GR (multilayer structure, GR sheets' islands size and their boundaries, impurities) can modify the outcome. It can be noted that in case of polycrystalline Ni, considered {111}, {011}, {001} orientations are most probable for surface formation due to the highest packing density. As was shown by preliminary calculations, structure of the planes with less packing density will transform into cluster type, where each cluster approximately represents the three most packed planes. It means that for the simulation of Ni polycrystalline structure it is necessary to average the characteristics of

3 different substrate orientations {111}, {011}, {001} taking into account some deviations in the areas when grain boundaries come to the surface.

5. Conclusions

Relaxation and reconstruction of Ni surface in {111}, {001}, {011} orientations with and without GR lamination at 300 K and 400 K was analyzed using molecular dynamic simulation. The simulation results show that in presence of GR, a higher packing density of substrate suppresses the structure modification in the plane with the surface, but rather allows the change in direction perpendicular to the surface. It was found that the substrate in {111} orientation provide the highest structural and thermal stability of GR/Ni system. Relaxation becomes more pronounced when the orientation of the substrate changes according to the sequence {111} → {001} → {011}, as such the maximum modification of the interplanar distance increases from 1 % to 6 %. Deposition of GR on Ni substrate in any orientation lowers the maximum interplanar distance change compared to the bulk for less than ~1 %. It was found that 400 K is the most suitable temperature for GR deposition on Ni, since it provides minimum structure changes. At this temperature the reconstruction of GR is taking place at all studied orientations of Ni substrate, which is manifested in the expansion of GR layers up to 0.2 % with increase of the average interatomic distance up to 0.6 % compared to the equilibrium state of GR. Crystallographic orientation of Ni substrate and temperature predetermine the surface roughness of GR/Ni system. The system formed by GR deposition on Ni {111} at 400 K is characterized by the least roughness.

Supplementary Materials: Not available.

Author Contributions: Sergiy Konorev – Simulation, Writing - original draft; Vitalii Yanchuk – Simulation, Writing - review; Ivan Kruhlov – Visualization, Formal analysis; Andrii Orlov – Calculated roughness parameters; Sergii Sidorenko – Issues, Conclusions; Igor Vladymyrskyi – Writing - review & editing; Sergey Prikhodko – Conceptualization, Supervision, Writing - review & editing; Svitlana Voloshko – Conceptualization, Supervision, Writing - Discussion.

Funding: This publication is based on work supported by grant #G-202108-68019 from the U.S. Civilian Research & Development Foundation (CRDF Global). Any opinions, findings, conclusions, or recommendations expressed in this material are those of the authors and do not necessarily reflect the views of CRDF Global.

Data Availability Statement: No new data were created or analyzed in this study. Data sharing is not applicable to this article.

Acknowledgments: Not available.

Conflicts of Interest: The authors declare no conflict of interest.

References

1. Balandin, A.A.; Ghosh, S.; Bao, W.; et al. Superior thermal conductivity of single-layer graphene, *Nano Lett.* **2008**, *8 (3)*, pp. 902-907. https://doi.org/10.1021/nl0731872
2. Chen, S.; Moore, A. L.; Cai, W.; et al. Raman measurements of thermal transport in suspended monolayer graphene of variable sizes in vacuum and gaseous environments, *ACS Nano* **2011** *5 (1)*, pp. 321-328. http://dx.doi.org/10.1021/nn102915x
3. Lim, S.; Park, H.; Yamamoto, G.; et al. Measurements of the electrical conductivity of monolayer graphene flakes using conductive atomic force microscopy, *Nanomater.* **2021**, *11 (10)* p. 2575. https://doi.org/10.3390/nano11102575
4. Fernández, S.; Molinero, A.; Sanz, D.; et al. Graphene-based contacts for optoelectronic devices, *Micromachines* **2020**, *11 (10)*, p. 919. https://doi.org/10.3390/mi11100919
5. Deshmukh, M.A.; Park, S.J.; Hedau, B.S.; Ha, T.J. Recent progress in solar cells based on carbon nanomaterials. *J. Sol. Energy* **2021**, *220*, pp. 953-990. https://doi.org/10.1016/j.solener.2021.04.001
6. Aepuru, R.; Aleksandrova, M.; Rao, Ch.N.; et al. Chapter 19 - Transparent conducting electrode materials for solar cell technologies. In Green Sustainable Process for Chemical and Environmental Engineering and Science. Solid State Synthetic Methods.; Eds: Boddula, I.R.; Asiri, A.M.; Rahman, M.M., Eds. Publisher: Elsevier, 2021; pp. 377-407. ISBN 9780128197202. https://doi.org/10.1016/b978-0-12-819720-2.00021-7
7. Muchuweni, E.; Mombeshora, E.T.; Martincigh B.S. and Nyamori V.O. Recent applications of carbon nanotubes in organic solar cells, *Front. Chem.* **2022**, *9*, p. 733552. https://doi.org/10.3389/fchem.2021.733552

8. Akhtaruzzaman, M.; Selvanathan, V.; Shahiduzzaman, M.; Hossain, M.I. Chapter 4 - Introduction to organic-inorganic hybrid solar cells. In Comprehensive guide on organic and inorganic solar cells: Fundamental concepts to fabrication methods.; Akhtaruzzaman, M.; Selvanathan, V. Eds.; Publisher: Academic Press, 2022; pp. 187-193, ISBN 9780323855297. https://doi.org/10.1016/B978-0-323-85529-7.00004-9
9. Chen, R.; Das, S.R.; Jeong, C.; et al. Co-percolating graphene-wrapped silver nanowire network for high performance, highly stable, transparent conducting electrodes, *Adv. Funct. Mater.* **2013**, *23*, pp. 5150-5158. https://doi.org/10.1002/adfm.201300124
10. Kruhlov, I.; Orlov, A.; Zakiev, V.; et al. Multi-layered thin-film metal contacts for new generation solar cells. In: TMS 2022 151st Annual Meeting & Exhibition Supplemental Proceedings, The Minerals, Metals & Materials Series; Publisher: *Springer, Cham.* **2022**, pp. 431-441. https://doi.org/10.1007/978-3-030-92381-5_39
11. Ding, J.; Zhao, H.; Wang, G.; et al. Interface modulations of high-performance graphene anticorrosion coatings, *Prog. Org. Coat.* **2023**, *178*, p. 107463. https://doi.org/10.1016/j.porgcoat.2023.107463
12. Al-Kuhaili, M.F. Electrical conductivity enhancement of indium tin oxide (ITO) thin films reactively sputtered in a hydrogen plasma, *J. Mater. Sci.: Mater. Electron.* **2020**, *31*, pp. 2729-2740. https://doi.org/10.1007/s10854-019-02813-9
13. Way, A.; Luke, J.; Evans, A.D.; et al. Fluorine doped tin oxide as an alternative of indium tin oxide for bottom electrode of semi-transparent organic photovoltaic devices, *AIP Adv.* **2019**, *9 (8)*, p. 085220. https://doi.org/10.1063/1.5104333
14. You, P.; Liu, Z.; Tai, Q.; et al. Efficient semitransparent perovskite solar cells with graphene electrodes, *Adv. Mater.* **2015**, *27 (24)*, pp. 3632-3638. https://doi.org/10.1002/adma.201501145
15. Yoon, J.; Sung, H.; Lee, G.; et al. Superflexible, high-efficiency perovskite solar cells utilizing graphene electrodes: towards future foldable power sources, *Energy Environ. Sci.* **2017**, *10*, pp. 337-345. https://doi.org/10.1039/C6EE02650H
16. Luo, Q.; Ma, H.; Hou, Q.; et al. All-carbon-electrode-based endurable flexible perovskite solar cells, *Adv. Funct. Mater.* **2018**, *28*, p. 1706777. https://doi.org/10.1002/adfm.201706777
17. Iqbal, M.Z.; Assad-Ur Rehman. Recent progress in graphene incorporated solar cell devices, *J. Sol. Energy* **2018**, *169*, pp. 634-647. https://doi.org/10.1016/j.solener.2018.04.041
18. Liu, X.; Wang, C.-Z.; Hupalo, M.; et al. Metals on graphene: interactions, growth morphology, and thermal stability, *Crystals* **2013**, *3 (1)*, pp. 79-111. https://doi.org/10.3390/cryst3010079
19. Yang, R.T.; Goethel, P.J.; Schwartz, J.M.; Lund, C.R.F. Solubility and diffusivity of carbon in metals, *J. Catal.* **1990**, *122 (1)*, pp. 206-210. https://doi.org/10.1016/0021-9517(90)90273-m
20. Chung, T.F.; Shen, T.; Cao, H.; et al. Synthetic graphene grown by chemical vapor deposition on copper foils, *Int. J. Mod. Phys. B* **2013**, *27 (10)*, p. 1341002. https://doi.org/10.1142/s0217979213410026
21. Cho, J. ; Gao, L.; Tian, J.; et al. Atomic-scale investigation of graphene grown on cu foil and the effects of thermal annealing, *ACS Nano* **2011**, 5 (5), pp. 3607-3613. https://doi.org/10.1021/nn103338g
22. Patel, Ch.R.P.; Awasthi, K.; Yadav, T.P. Selective growth of uniform graphene films on metallic (Cu and Au) substrates, *J. Int. Acad. Phys. Sci.* **2022**, *26 (2)*, pp. 175-184. https://www.iaps.org.in/journal/index.php/journaliaps/article/view/940
23. Kiraly, B.; Iski, E.V.; Mannix, A.J.; et al. Solid-source growth and atomic-scale characterization of graphene on Ag(111), *Nat. Commun.* **2013**, *4*, p. 2804. https://doi.org/10.1038/ncomms3804
24. Cheianov, V.V.; Fal'ko, V.I. Selective transmission of dirac electrons and ballistic magnetoresistance of N−P junctions in graphene, *Phys. Rev. B* **2006**, *74 (4)*, p. 041403. https://doi.org/10.1103/physrevb.74.041403
25. Giovannetti, G.; Khomyakov, P. A.; Brocks, G.; et al. Doping graphene with metal contacts, *Phys. Rev. Lett.* **2008**, *101 (2)*, p. 026803. https://doi.org/10.1103/physrevlett.101.026803
26. Dahal, A.; Batzill, M. Graphene–nickel Interfaces: a review, *Nanoscale* **2014**, *6 (5)*, p. 2548. https://doi.org/10.1039/c3nr05279f
27. Xiao, W.; Baskes, M.I.; Cho, K. MEAM Study of Carbon Atom Interaction With Ni Nano Particle, *Surf. Sci.* **2009**, *603 (13)*, pp. 1985-1998. https://doi.org/10.1016/j.susc.2009.03.009
28. LAMMPS Molecular Dynamics Simulator. Available online: www.lammps.org (accessed on 17.08.23).
29. Kittel, Ch.; Introduction to Solid State Physics, Publisher: *Wiley India Pvt Ltd*, **2012**. ISBN-10 : 9788126535187
30. Gao, Y.; Lihua, L.; et al. Structure of Graphene and Its Disorders: A Review. *Sci. Technol. Adv. Mater.* **2018**, *19 (1)*, pp. 613–648. https://doi.org/10.1080/14686996.2018.1494493
31. Rankin, D. CRC handbook of chemistry and physics, 89th edition, edited by David R. Lide. *Crystallogr. Rev.*, **2009**, *15 (3)*, pp. 223-224. https://doi.org/10.1080/08893110902764125
32. Barron, T. H. K.; White, G. Heat Capacity and Thermal Expansion at Low Temperatures. Publisher: Springer New York, **1999**. ISBN 978-0-306-46198-9. https://doi.org/10.1007/978-1-4615-4695-5
33. Engelmann, Y.; Bogaertsb, A.; Neyts, E.C. Thermodynamics at the Nanoscale: Phase Diagrams of Nickel–carbon Nanoclusters and Equilibrium Constants for Phase Transitions, Nanoscale **2014**, *6 (20)*, pp. 11981–11987. https://doi.org/10.1039/c4nr02354d

34. Frenken, J.W.M.; Smeenk, R.G., Van der Veen, J.F. Static and dynamic displacements of nickel atoms in clean and oxygen covered Ni(001) surfaces, *Surf. Sci.* **1983**, *135 (1-3)*, pp. 147-163. https://doi.org/10.1016/0039-6028(83)90216-9
35. Feidenhans'l, R.; Sørensen, J.E.; Stensgaard, I. Surface relaxation of Ni(110) investigated by high energy ion scattering, *Surf. Sci.* **1983**, *134 (2)*, pp. 329-337. https://doi.org/10.1016/0039-6028(83)90427-2
36. Manasoglu, G.; Celen, R.; Akgun, M.; Kanik, M. The Effect of Graphene Coating on Surface Roughness and Friction Properties of Polyester Fabrics, *Mater. Sci.* **2021**, *27 (4)*, pp. 470-476. https://doi.org/10.5755/j02.ms.27903
37. Kumar, H. G. P.; Xavior, M. A. Effect of graphene addition and tribological performance of Al 6061/graphene flake composite, *Tribol. Mater. Surf. Interfaces* **2017**, *11 (2)*, pp. 88-97. https://doi.org/10.1080/17515831.2017.1329920
38. Kruhlov, I.O.; Vladymyrskyi, I.A.; Dubikovskyi, O.; et al. Reduction processes in Ni/Cu/Cr/Si(100) thin films under low-energy Ar+ ion bombardment. *Mater. Res. Express* **2020**, *6 (№12)*, p. 126431. https://doi.org/10.1088/2053-1591/ab6382
39. Ren, S.; Cui, M.; Liu, C.; Wang, L. A comprehensive review on ultrathin, multi-functionalized, and smart graphene and graphene-based composite protective coatings. *Corrosion Sci.* **2023**, *212*, p. 110939. https://doi.org/10.1016/j.corsci.2022.110939
40. Ding, J.; Zhao, H.; Wang, G.; Wang, J.; Zhu, J. Interface modulations of high-performance graphene anticorrosion coatings. *Prog. Org. Coat.* **2023**, *178*, p. 107463. https://doi.org/10.1016/j.porgcoat.2023.107463